ENHANCED KNOWLEDGE IN SCIENCES AND TECHNOLOGY
e-ISSN: 2773-6385

EKST

Vol. 5 No. 1 (2025) 162-171
https://publisher.uthm.edu.my/periodicals/index.php/ekst

Green Synthesis of Hydroxyapatite from Oyster Shell Waste for Catalytic Applications

Adibah Rahmat[1], Izat Yahaya[2], Hana Fareeha Azizuddin[1], Hanis Imran Hisham[1], Muhammad Azizi Najmi Mamat Ali[1], Nodiana Mohamad[1], Nur Aqilah Abdullah[1], Nur Nadirah Muhammad Sukri[1], Vyranath Ko Mon[1], Riana Rayner[1]

[1] *Department of Physics and Chemistry, Faculty of Applied Sciences and Technology, UTHM Kampus Cawangan Pagoh, Hab Pendidikan Tinggi Pagoh, KM 1, Jalan Panchor, 86400 Pagoh, Muar, Johor, MALAYSIA.*

[2] *Centre for Diploma Studies, UTHM Kampus Cawangan Pagoh, Hab Pendidikan Tinggi Pagoh, KM 1, Jalan Panchor, 86400 Pagoh, Muar, Johor, MALAYSIA.*

*Corresponding Author: yahizat@uthm.edu.my
DOI: https://doi.org/10.30880/ekst.2025.05.01.021

Article Info

Received: 3 June 2025
Accepted: 26 June 2025
Available online: 30 July 2025

Keywords

Oyster shell, Hydroxyapatite, Cr (III) Removal

Abstract

The synthesis of hydroxyapatite from oyster shells was accomplished using a calcination process to transform calcium carbonate ($CaCO_3$) into calcium oxide (CaO), followed by hydrothermal treatment which facilitated the formation of highly crystalline hydroxyapatite with controlled morphology and improved purity suitable for catalytic applications. Characterization techniques, including Scanning Electron Microscopy (SEM), Energy Dispersive X-ray Spectroscopy (EDX), X-ray Diffraction (XRD), and Fourier Transform Infrared Spectroscopy (FTIR), confirmed the formation of hydroxyapatite, while the catalytic application was studied using UV-Vis spectroscopy. SEM images revealed a granular, clustered morphology, while EDX analysis indicated the presence of calcium, phosphorus, and oxygen, consistent with hydroxyapatite's expected composition. XRD patterns displayed characteristic hydroxyapatite peaks, and FTIR spectra confirmed the presence of phosphate groups. The synthesized hydroxyapatite demonstrated high catalytic efficacy in removing Cr(III) from an aqueous $Cr(NO_3)_3$ solution, achieving an 82.12% removal efficiency, reducing the concentration from 850 ppm to 152 ppm within 3 hours. These results highlight hydroxyapatite's potential in environmental remediation applications. Further optimization of synthesis conditions, alongside studies on catalyst regeneration and scalability, is recommended to enhance material performance and practical applicability.

1. Introduction

Hydroxyapatite (HAP) ($Ca_{10}(PO_4)_6(OH)_2$) is a calcium phosphate ceramic part of the apatite family. It is the primary inorganic constituent of bone and teeth, playing a crucial role in their firmness and durability. This bioactive ceramic is ideal for load-bearing applications due to its robust mechanical properties and exceptional biocompatibility, making it a preferred material in orthopaedic applications [1][2]. Hydroxyapatite can integrate seamlessly with bone, avoiding local toxicity or inflammation, which underscores its importance in medical

applications [1][2]. Recent advancements have further extended its applications, revealing its potential as an environmentally friendly catalyst in various chemical reactions [4]. Hydroxyapatite's flexibility and multifunctionality allow for numerous modifications that enhance its catalytic performance in specific reactions, making it a highly versatile and effective catalyst.

Oyster shells, primarily composed of calcium carbonate (98%), are an abundant and cost-effective natural waste material with minimal impurities [3]. Their chemical composition makes them particularly attractive for converting biological material into hydroxyapatite (HA) powders [3]. Using oyster shells as a calcium source for HAP production effectively reduces the high costs and environmental impacts of traditional methods [4][5]. By transforming calcium carbonate into calcium oxide (CaO) for HAP synthesis, this approach leverages a plentiful and eco-friendly resource. Recycling oyster shells not only lowers raw material expenses but also reduces landfill waste, making the process more sustainable [11]. This green synthesis method produces high-quality HA economically, providing a viable alternative to conventional production techniques.

Chromium (III) compounds, such as chromium (III) oxide and chromium (III) nitrate, are widely used in various industries. Chromium (III) oxide imparts a green colour to products like cement, rubber, tiles, and ceramics, while chromium (III) nitrate serves as a dye and coating material [19]. The discharge of industrial wastewater containing Cr (III) into aquatic environments results in toxic effects on aquatic life and leads to the accumulation of Cr (III) in soil [19]. This accumulation adversely affects plant growth by inhibiting photosynthetic enzymes, causing imbalances and reduced agricultural yields [19]. Consequently, there is a critical need to develop methods for removing chromium from wastewater prior to environmental release. One approach involves the use of hydroxyapatite, which acts as both a catalyst and an adsorbent for the removal of chromium (III) from water [4]. The objectives of this study are to synthesize HAP from waste oyster shells, characterize the hydroxyapatite using scanning electron microscopy (SEM), Fourier-transform infrared spectroscopy (FTIR), energy-dispersive X-ray spectroscopy (EDX), and X-ray diffraction (XRD), and evaluate its efficacy in the removal of chromium (III) from wastewater. This study demonstrated significant potential, particularly in its ability to achieve effective removal of high concentrations of Chromium (III) within a relatively short duration of only three hours.

2. Materials and Methods

This study was conducted with Phosphoric acid, (H_3PO_4, 85%) and Sodium Hydroxide (NaOH, 98%) were supplied by Sigma Aldrich. Chromium nitrate, $Cr(NO)_3$ was also supplied by Sigma Aldrich.

2.1 Synthesis of Calcium Oxide (CaO)

Oyster shells were collected from the river of Muar, Johor. The shells were thoroughly purified, which included multiple washes with distilled water to remove the impurities. Then, the cleaned shells were dried in oven at a consistent temperature of 80°C for 24 hours [3]. The dried oyster shells were crushed using a hammer, then refined with a pestle and mortar to reduce the shells to smaller sizes. The crushed shells were milled and sieved to produce a powdery consistency with particles smaller is 0.075mm. Next, the $CaCO_3$ was heated at 1200°C in a furnace for 2 hours with the temperature was gradually increased at rate of 5°C per minute, to create a CaO [3].

2.2 Synthesis of Hydroxyapatite (HAP)

A calcium oxide (CaO) solution with a concentration of 1 mol/L was prepared. CaO powder was weighed and put into 2 L beaker. Then, distilled water was filled into the beaker until it reached 1 L of the beaker. A magnetic stirrer was inserted into the beaker and the beaker was placed on the hot plate. The hot plate was turned on and the solution was stirred until white suspension presented. To prepare 0.6 mol of phosphoric acid, H_3PO_4 85% H_3PO_4 was poured into 1 L volumetric flask. Volumetric flask was filled with distilled water for 1 L to obtain 0.6 mol H_3PO_4. After that, 0.6 mol H_3PO_4 was added drop by drop into the CaO solution while stirring the solution. During the addition of H_3PO_4 into CaO solution, sodium hydroxide, NaOH was used to maintain the pH of the solution. After adding 1 L of H_3PO_4, the mixture was continued to stirred for 2 hours to obtain opaque white suspension in the solution. The solution was left for overnight in the laboratory. The solution formation was illustrated by equation (1) [3].

$$10Ca(OH)_2 + 6H_3PO_4 \rightarrow Ca_{10}(PO_4)_6(OH)_2 + 18H_2O \quad (1)$$

Then, the solution was filtered by using vacuum pump to remove the water molecule formed in the mixture and obtain the white suspension in the solution. The solid obtained was dried in the oven at 105℃ for 2 hours. After that, the dry solid was transformed into powder form via mortar. Then, the powder was furnace once again at 600℃ for 2 hours [3].

Enhanced Knowledge in Sciences and Technology Vol. 5 No. 1 (2025) p. 162-171

2.3 Fourier Transform Infrared (FTIR) Spectroscopy

Fourier Transform Infrared Spectroscopy (FTIR) was used to analyse the functional groups present in the oyster shell samples before and after calcination and in the synthesized hydroxyapatite (HAP). The FTIR spectrometer used in the analysis had a wavenumber range of 4000 - 1000 cm^{-1}. The spectral analyses helped in identifying the various functional groups and confirming the chemical transformations of the oyster shells through the different stages of processing.

2.4 Scanning Electron Microscopy (SEM) and Energy Dispersive X-ray (XRD) Analysis

Scanning Electron Microscopy (SEM) used for analysing samples of calcium oxide (CaO), calcium carbonate ($CaCO_3$), and hydroxyapatite (HAP) powder, the samples first underwent a drying process to ensure accurate and high- quality images. The samples were placed in an oven set at 60-70°C for one day to remove any residual moisture. Then, the SEM stubs were cleaned with acetone to remove contaminants before being fitted with double-sided carbon conductive tapes. A small amount of each powder was mounted on separate carbon conductive tapes. Before coating the samples with a thin layer of gold (Au), the samples were blown to remove any excess powder on the carbon conductive tapes. The prepared samples were then placed into the SEM chamber. The SEM software was used to capture high-resolution images to analyse the morphology and particle size of CaO, $CaCO_3$, and HAP. Additionally, Energy Dispersive X-ray Analysis (EDX) software was used to determine the elemental composition of the samples.

2.5 X-ray Diffraction (XRD) Analysis

Calcium Oxide (CaO) was ground into a fine powder using a mortar and pestle. The powders were extensively blended to achieve consistency. A small quantity of CaO powder was placed on the XRD sample holder. A flat plate was employed to compress and even out the powder to achieve a flat surface. Once the instrument was calibrated and prepared, the XRD analysis was conducted. Information was gathered through a 2θ scan range. The procedure was observed, and CaO peaks were found. Peak shape and intensity analysis were used to assess the sample's crystallinity and purity. The results were evaluated in comparison to standard industry reference patterns. The procedure was performed again for the analysis of Calcium Carbonate ($CaCO_3$) and hydroxyapatite (HAP).

2.6 Calibration Curve of Chromium III Solution

Prepare chromium (III) solution from stock of chromium nitrate, Cr(NO)3 which has a concentration of 1000 ppm. Create a standard solution for the chromium (III) solution by diluting the stock to obtain eight different concentrations, 50, 100, 150, 200, 250, 300, 350, and 400 ppm. The absorbance of these concentrations is measured by using UV- Visible Spectrophotometer. Plot a graph showing the relationship between absorbance and concentration. Fig. 1 illustrates the calibration curve of chromium (III) solution at 408 nm [22]. A calibration curve showing the relationship between absorbance and concentration of chromium (III) solution. Following that, the concentration of the unknown chromium (III) solution was calculated using Beer-Lambert's law as stated in equation (2).

$$A = \varepsilon lc \tag{2}$$

Where A is the absorbance, l is the optical path length of the cell (cm), ε is the molar absorption coefficient ($M^{-1}cm^{-1}$).

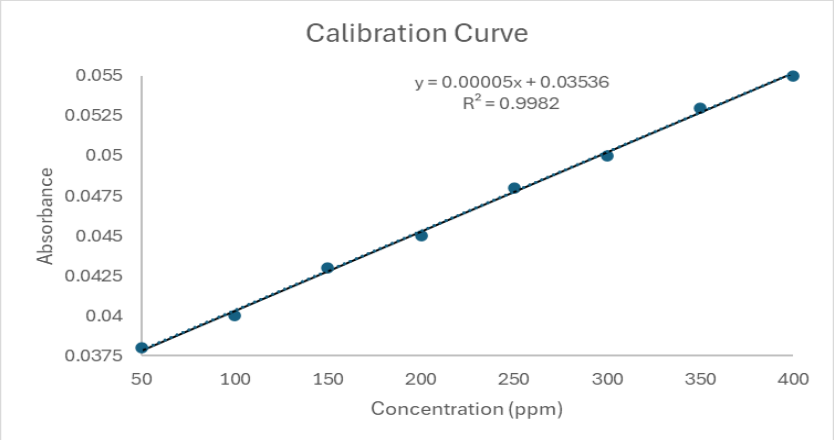

Fig. 1 Calibration curve of chromium (III) solution

2.7 Adsorption Rate

About 10 mg of hydroxyapatite is weighed and placed in the beaker and add 10 mL of 800 ppm of chromium (III) solution prepared before. The solution then is shacked for 3 hours at 120 rpm in water bath at room temperature. The absorbance of after treated with hydroxyapatite is measured using UV-Visible Spectrophotometer at 408 nm. The amount of chromium absorbed can be calculated using Langmuir isotherm equation as stated in equation (3) [22].

After treated the chromium with hydroxyapatite, the concentration unknown chromium (III) solution can be determined by using Beer Lambert law formula as shown in equation (2), where A is the absorbance, ε is the molar absorptivity, l is the path length and c is the concentration of chromium (III) solution.

$$q_e = \frac{(C_i - C_f).V}{W} \quad (3)$$

Where q_e is the amount of chromium (III) absorbed (ppm), C_i is the initial concentration of chromium (III) solution, C_f is the final concentration of chromium (III) solution, V is the volume of chromium (III) solution (L) and W is the mass of hydroxyapatite (g) [1].

3. Result and Discussion

3.1 Fourier Transform Infrared (FTIR) Spectroscopy

In Fig. 2, the chemical structure of Hydroxyapatite is shown. Fig. 3 shows the FTIR spectra analysis was performed to identify the various functional groups that present on the oyster shell before calcination ($CaCO_3$), oyster shell after calcination (CaO) and hydroxyapatite (HPA). The FTIR spectra was recorded in the range of 500-4000cm-1.

The FTIR spectrum of the oyster shell shows the fundamental bands, which are sharp, broad and stronger, stretching at 1406, 883 and 714cm^{-1}, indicating the presence of $CaCO_3$. The peak stretching at 1406 cm-1 is characteristics of the C-O bond, showing a bond between oxygen atom of carbonate and calcium atom. Additionally, the sharp band at 883 and 714 cm-1 indicates to the bending of carbonate (CO_3^{2-}), proving that oyster shell is predominantly made of calcium carbonate ($CaCO_3$). This peak corresponds with the findings by [3], who observed comparable carbonate peaks in the FTIR spectra of oyster shells.

After calcination, the peaks decrease, observing of CaO, show a broad peak at 877cm^{-1}, which is bending of carbonate (CO_3^{2-}), where it indicates the carbonation of calcium oxide. This indicates the formation of calcium oxide (CaO) as a result of the decomposition of calcium carbonate ($CaCO_3$) during the calcination process, as evidenced by the characteristic peaks observed in the FTIR analysis of the CaO powder [3].

Next, FTIR spectrum of synthesized HAP shows the prominent peaks at 1407, 1078, 1016, 965, 626, 603 and 559 cm^{-1}. The weak band at 1407 cm^{-1} indicates the presence of bending vibrations associated with carbonate group suggesting that carbon from organic matter was not fully pyrolyzed and may have been incorporated into the HA crystal structure. The bands in the peaks at 1078, 1016, and 965 cm-1 corresponds to the asymmetric stretching of phosphate group of HAP *(PO_4^{-3})* while the bands at peaks 626, 603 and 559 are attributed to the bending of phosphate group of HAP *(PO_4^{-3})*. The presence of these peaks confirms the formation of hydroxyapatite, characterized by its distinct phosphate groups. The present findings are similar with previous studies, who indicate the FTIR spectra of hydroxyapatite [3].

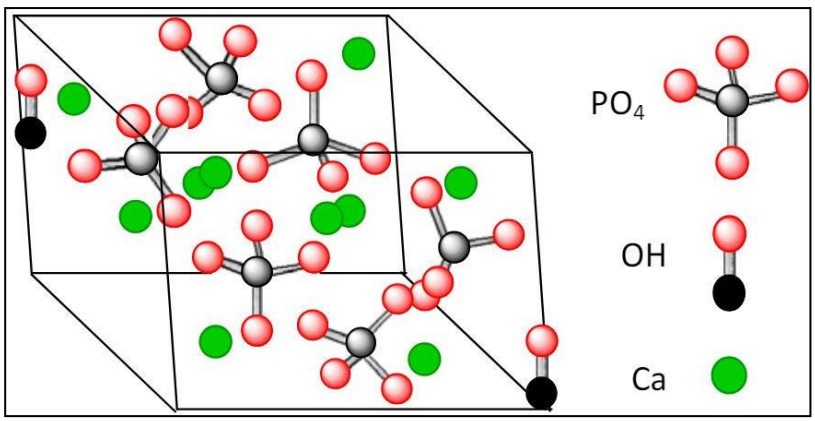

Fig. 2 Chemical Structure of Hydroxyapatite [32]

Enhanced Knowledge in Sciences and Technology Vol. 5 No. 1 (2025) p. 162-171

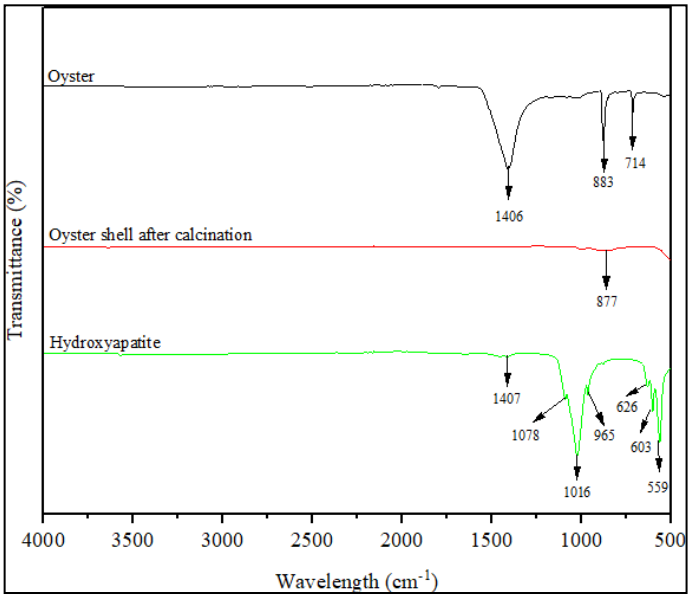

Fig. 3 FTIR spectra of oyster shell before calcination ($CaCO_3$), oyster shell after calcination (CaO), and hydroxyapatite (NHA)

3.2 Morphology Analysis

Scanning electron microscopy (SEM) was employed to characterize surface morphology and particle sizes of the hydroxyapatite (HAP) samples that act as catalyst. The oyster shell samples ($CaCO_3$) before furnace was shown at Fig. 4(a). The SEM displays the image of $CaCO_3$ that had crystalline structure, with particles forming rhombohedral shapes, which was the morphology of calcite [25]. The calcite crystalline structure is stable, which can contribute to the durability and reusability of the catalyst. After the furnace of $CaCO_3$, CaO was shown in Fig. 4(b). The SEM image of CaO shows irregularly shaped particles with sharp edges and smooth surfaces. The surface area of CaO has direct impact on its catalytic activity; hence the higher surface area catalyst is expected to have higher catalytic activity [26]. These structural characteristics are essential for understanding CaO reactivity in chemical processes. The SEM image of HAP in Fig. 4(c) illustrates rod-shaped particles. It can possess a high surface area to volume ratio, which enhances their reactivity and interaction with other substances, making them particularly useful in catalysis and adsorption.

The energy-dispersive X-ray (EDX) spectra was to analyse the three substances that was calcium carbonate ($CaCO_3$), calcium oxide (CaO), and hydroxyapatite (HAP). The peak intensities of each element were analysed to determine the composition of the samples. The EDX spectrum showed a significant peak for calcium, consistent with the expected presence of calcium carbonate ($CaCO_3$) [3]. Additionally, the presence of carbon and oxygen aligned well with the chemical formula of $CaCO_3$. In Fig. 4(d), the EDX results for the oyster shells indicate that $CaCO_3$ consists of a high percentage of calcium carbonate. The EDX analysis shows that $CaCO_3$ contains 30.07% calcium, 28.73% carbon, and 41.20% oxygen by weight. The weight percentages show oxygen as the most abundant element, followed by calcium and carbon, which is typical for $CaCO_3$, where oxygen atoms substantially contribute to the mass due to their presence in both the carbonate ion and the overall compound. The absence of carbon clearly indicated the conversion from $CaCO_3$ to CaO, confirming that the sample primarily consisted of calcium oxide [3].

In Fig. 4(e), the chemical composition of CaO prepared from burning oyster shells, as shown by EDX analysis, indicated that CaO consisted of calcium (Ca) and oxygen (O). The analysis showed that CaO contained 56.89% calcium and 43.11% oxygen by weight. The weight and atomic percentages revealed a higher proportion of calcium compared to the EDX results for $CaCO_3$, which was consistent with the removal of CO_2 (carbon dioxide) during the calcination process, leaving behind CaO. The EDX spectrum for hydroxyapatite showed the presence of calcium, phosphorus, and oxygen. The significant presence of phosphorus alongside calcium and oxygen was indicative of the hydroxyapatite structure, which included phosphate groups (PO_4^{3-}) [3]. As for the hydroxyapatite (HAP) powder prepared from the reaction of Ca $(OH)_2$ with H_3PO_4, its chemical composition, shown in Fig. 4(f), indicated that HAP contained 28.39% calcium, 13.72% phosphorus, and 57.89% oxygen by weight. The higher oxygen content by atomic percentage aligned with the hydroxyapatite formula, which contained a substantial amount of oxygen due to the phosphate and hydroxyl groups in its structure.

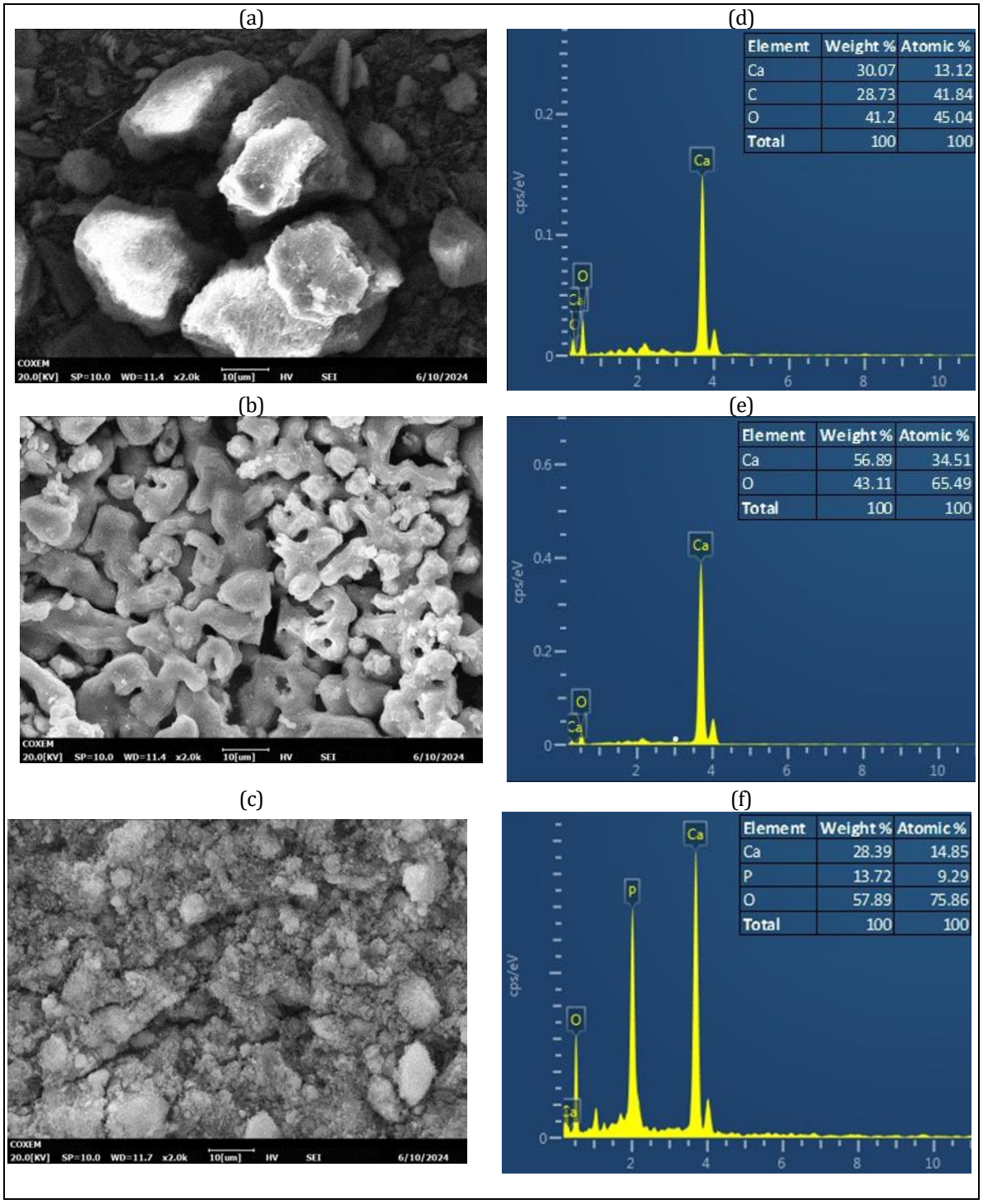

Fig. 4 (a) SEM images of CaCO3 (b) SEM images of CaO, (c) SEM images of HAP, (d) EDX spectra of CaCO3, (e) EDX spectra of CaO, (f) EDX spectra of HAP

3.3 X-ray Diffraction (XRD) Analysis

The XRD analysis of CaO in Fig. 5(a) revealed distinct peaks with 2θ values of 31.956, 37.203, and 53.703. These values aligned with the crystallographic planes (111), (200), and (220) [3] and suggested a cubic crystalline structure. Strong diffraction from the (200) plane was indicated by the greatest intensity peak at 53.703, which verified the sample's good crystallinity and phase purity. A well-ordered crystal lattice was revealed by the sharp and well-defined peaks. The sample's identification and structural consistency are confirmed by the close alignment of peak positions and relative intensities with the reference XRD pattern [3]. The efficiency of XRD in verifying the crystalline structure and phase purity of CaO was shown by this analysis.

Fig. 5(b) showed an XRD pattern of with seven distinct peaks at 2θ (22.755, 29.216, 35.676, 39.129, 42.516, 47.260, and 48.318). These values suggested a cubic crystalline structure and aligned with the crystallographic

Enhanced Knowledge in Sciences and Technology Vol. 5 No. 1 (2025) p. 162-171

planes (002), (104), (116), (018) and (004) [3]. The similarity in diffraction peak positions and intensities to the reference XRD data [3] indicates the successful identification and stable crystal structure of $CaCO_3$.

The XRD pattern of HAP was shown in Fig. 5(c), and it included numerous sharp peaks that aligned with the crystallographic planes (002), (210), (211), (310), (222), (213), and (321) [3]. This indicated that HAP had a high degree of crystallinity. Peaks (25.536, 31.542, 32.577, 33.82029.550, 46.316, and 49.215) were observed at 2θ. The sample's high crystallinity and phase purity were confirmed by the maximum intensity peak at 49.215, which indicated strong diffraction from the (211) plane. The identification and structural consistency of HAP were demonstrated by the close matching of peak positions and relative intensities with the reference XRD pattern [3].

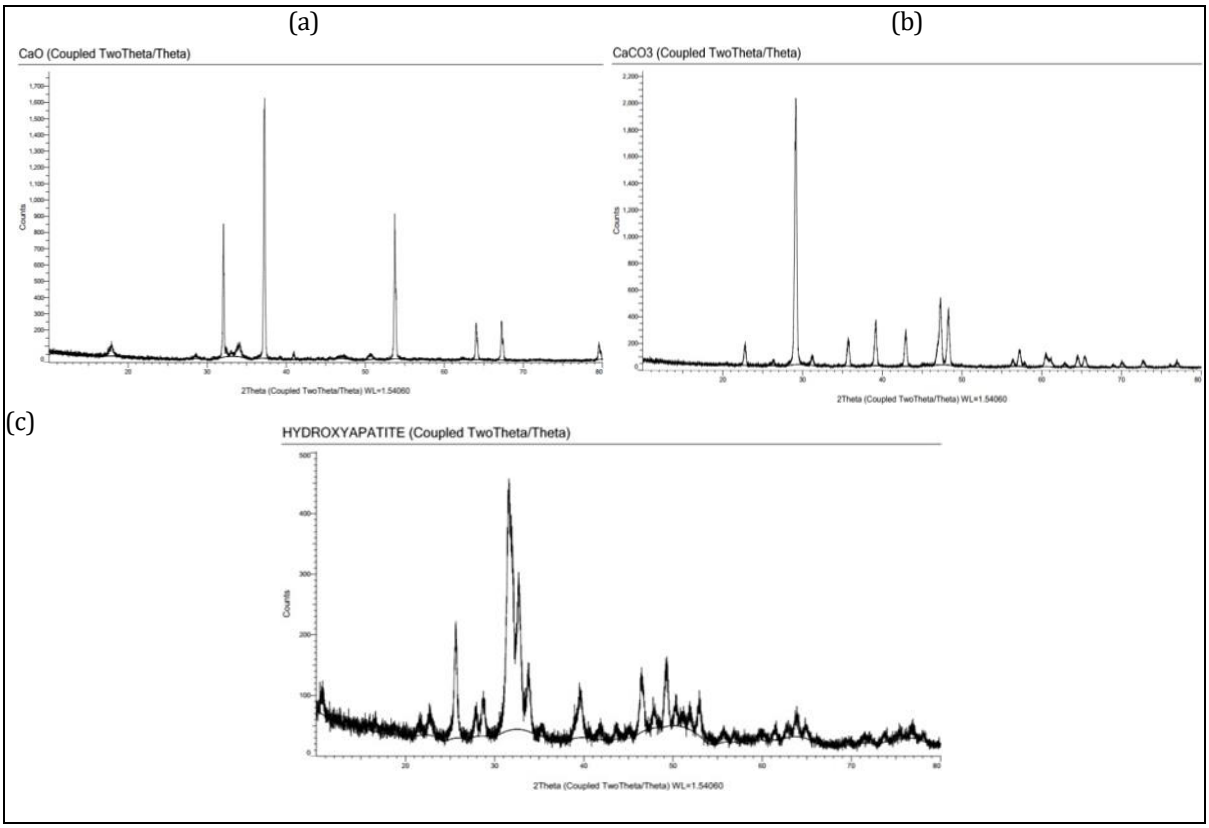

Fig. 5 (a) XRD images of CaO, (b) XRD images of CaCO3, (c) XRD images of HAP

3.4 Effect of pH on Hydroxyapatite

The precipitation of HAP from digested CaCO3 was observed at pH 8-12. The FTIR spectra in Fig. 3 of all samples have shown bands corresponding to HAP structure. Similarly, the results from XRD patterns in Fig. 5 have shown that the samples underwent a pure apatite phase, and the sharp peaks confirm that they were well crystallized. It indicated that the different selections of pH value (pH 8-12) were successful to prepare HAP by digested $CaCO_3$. Studies on the precipitation behaviour of calcium phosphates, considering calcium and phosphate ion concentrations at constant ionic strength, have shown that no precipitation occurs at pH 6. However, at pH values exceeding 7.4, the formation of hydroxyapatite (HAP) is thermodynamically favourable. CaCO3 was unstable under acidic pH conditions, but reaction with phosphoric acid produces poorly soluble monetize coatings which block further reaction [33].

Furthermore, HAP was formed at basic pH levels, where CaCO3 was stable, and no reaction was expected unless the system was heated under pressure such as takes place in the hydrothermal process. At ambient pressure, hydrogen phosphate groups were first absorbed on the carbonate surface, and then were deprotonated to form calcium orthophosphate, releasing the carbonate ions into the solution [31].

The synthetic HAP using H3PO4 as phosphate sources reacted with the digested CaCO3 at pH 9 obtained after phosphates as a function of the concentration of the calcium ions, phosphate ions and the pH at constant ionic force at pH = 6 there is no precipitation, and at a pH higher than 7.4 it is feasible that HAP will precipitate [33]. One must recall the following facts: CaCO3 was unstable under acidic pH conditions, but reaction with phosphoric acid produces poorly soluble monetize coatings which block further reaction shown in Fig. 6.

Fig. 6 HAP precipitate after vacuum

3.5 Adsorption of Chromium (III)

The absorption of calcium hydroxyapatite in removing chromium (III) solution were evaluated by measuring the absorbance of the solution before and after treatment using UV-vis spectroscopy. Initially, the chromium (III) solution's absorbance was recorded at 0.078 and after treatment with calcium hydroxyapatite was 0.043, which is greatly decreased. The significant change of absorbance can be determined by identifying the initial and final concentration of both before and after treatment using Equation (1) which are 852.8 ppm and 152.8 ppm respectively. The equilibrium adsorption capacity after the treatment was determined using Equation (2) which is 82.12%.

In this study, the experiment was conducted to observe the efficiency of the hydroxyapatite, HA as catalyst in removing chromium (III) ions from its solution. This is due to the previous study that had stated that the physico-chemical features of the HA compounds will enhance the removal of the toxic metal ions from wastewater through mechanisms of ion exchange and dissolution-precipitation [18]. HA shows its catalytic properties as it provided active surfaces for adsorption process. Its presence would help in enhancing the adsorption of the toxic metal ions from wastewater [19].

In this reaction, both mechanisms were involved where the toxic metal ions in chromium (III) solution will be replaced with calcium ions in HA structures. The hydroxyl and phosphate groups in HA will facilitate the mechanism as they contributed to high affinity of the HA compounds. The toxic metal ions will react with phosphate ions and form chromium phosphate where these compounds were insoluble and will form the precipitate from this reaction. This can be proven through equation (4) [20].

$$Ca_{10}(PO_4)_6(OH)_2 + 2Cr^{3+} \rightarrow Ca_7Cr_2(PO_4)_6(OH)_2 + 3Ca^{2+} \quad (4)$$

As shown in equation, the formation of the new compound which was chromium hydroxyapatite indicated that the chromium (III) ions had been combined into HA structure which leading to precipitation of chromium phosphate. The calcium ions were released from HA compounds in this reaction and produced as safer byproducts compared to chromium (III) ions [22]. This reaction can be evidenced through UV-Vis Spectroscopy analysis were based on the result, there were changes in absorbance peaks for presence of the chromium (III) ions. It showed the final concentration of chromium (III) solution after the HA reaction much lower than before mixing with HA compounds.

4. Conclusion

In conclusion, the synthesis of hydroxyapatite from oyster shells was successfully achieved through calcination to convert calcium carbonate ($CaCO_3$) to calcium oxide (CaO), followed by hydrothermal treatment. Comprehensive characterization using SEM, EDX, XRD, and FTIR confirmed the formation of hydroxyapatite. SEM images revealed a granular, clustered morphology typical of hydroxyapatite, while EDX analysis identified the presence of calcium, phosphorus, and oxygen, consistent with the expected composition. XRD patterns displayed characteristic peaks of hydroxyapatite, and FTIR spectra corroborated the presence of phosphate groups. The synthesized hydroxyapatite exhibited high efficacy as a catalyst in removing Cr(III) from an aqueous $Cr(NO_3)_3$ solution, reducing the concentration from 850 ppm to 152 ppm within 3 hours, corresponding to an 82.12% removal efficiency. This significant reduction underscores hydroxyapatite's potential for environmental remediation applications. In conclusion, further optimization of synthesis conditions, alongside studies on catalyst regeneration and scalability, is recommended to enhance material performance and practical applicability. Applying the synthesized hydroxyapatite to real wastewater systems and exploring the adsorption kinetics would help in understanding its practical applicability. Moreover, considering the feasibility of scaling up the synthesis process may support its transition from laboratory-scale experiments to real-world applications in water treatment technologies.

Acknowledgement

The authors would like to acknowledge the support of the Pusat Pengurusan Makmal Kampus Cawangan Pagoh Universiti Tun Hussein Onn Malaysia (UTHM), for providing the research facilities.

References

[1] Hossain, S. S., & Roy, P. K. (2020). Sustainable ceramics derived from solid wastes: a review. *In Journal of Asian Ceramic Societies*,8(4), pp. 984–1009). https://doi.org/10.1080/21870764.2020.1815348
[2] Filip, D. G., Surdu, V. A., Paduraru, A. V., & Andronescu, E. (2022). Current Development in Biomaterials—Hydroxyapatite and Bioglass for Applications in Biomedical Field: A Review. *In Journal of Functional Biomaterials* 13(4). MDPI. https://doi.org/10.3390/jfb13040248
[3] Aljaberi, K., AlBadr, R. M., & Ziadan, K. M. (2022). A new approach to prepare nano hydroxyapatite from oyster shells used for dental applications. *Journal of Kufa-Physics*, *14*(02),35 46. https://doi.org/10.31257/2018/jkp/2022/140205
[4] Yook, H., Hwang, J., Yeo, W., Bang, J., Kim, J., Kim, T. Y., Choi, J. S., & Han, J. W. (2023). Design Strategies for Hydroxyapatite-Based Materials to Enhance Their Catalytic Performance and Applicability. *Advanced materials (Deerfield Beach, Fla.),* 35(43), e2204938. https://doi.org/10.1 002/adma.202204938
[5] Ebrahimi, S., Nasri, C. S. S. M., & Arshad, S. E. B. (2021). Hydrothermal synthesis of hydroxyapatite powders using Response Surface Methodology (RSM). *PloS One*. https://doi.org/10.1371/journal.pone.0251009
[6] Mohd Pu'ad, N. A. S., Koshy, P., Abdullah, H. Z., Idris, M. I., & Lee, T. C. (2019). Syntheses of hydroxyapatite from natural sources. *In Heliyon Elsevier Ltd,* 5(5) https://doi.org/10.1016/j.heliyon. 2019.e01588
[7] Topić Popović, N., Lorencin, V., Strunjak-Perović, I., & Čož-Rakovac, R. (2023). Shell Waste Management and Utilization: Mitigating Organic Pollution and Enhancing Sustainability. *In Applied Sciences (Switzerland)*
[8] 13(1). MDPI. https://doi.org/10.3390/app13010623
[9] Rial, R., González-durruthy, M., Liu, Z., & Ruso, J. M. (2021). Advanced materials based on nanosized hydroxyapatite. *In Molecules* 26(11). MDPI AG. https://doi.org/10.3390/molecules26113190
[10] Baino, F., Schwentenwein, M., & Verné, E. (2022). Modelling the Mechanical Properties of Hydroxyapatite Scaffolds Produced by Digital Light Processing- Based Vat Photopolymerization. *Ceramics.* https://doi.org/10.3390/ceramics5030044
[11] Kokubo, T., & Takadama, H. (2006). How useful is SBF in predicting in vivo bone bioactivity? *Biomaterials,*
[12] 27(15), 2907–2915. https://doi.org/10.1016/j.biomaterials.2006.01.017
[13] Dorozhkin, S. V. (2010). Bioceramics of calcium orthophosphates. *Biomaterials,* 31(7), 1465–1485. https://doi.org/10.1016/j.biomaterials.2009.11.050
[14] Taguas, E. V., Marín-Moreno, V., Díez, C. M., Mateos, L., Barranco, D., Mesas-Carrascosa, F. J., Pérez, R., García-Ferrer, A., & Quero, J. L. (2021). Opportunities of super high-density olive orchard to improve soil quality: Management guidelines for application of pruning residues. *Journal of Environmental Management*, 293, 112785. https://doi.org/10.1016/j.jenvman.2021.112785
[15] Bi, W., Sun, S., Bei, S., & Jiang, Y. (2020, March). Segregation of S at Mo(001)/MoSi2(001) interface.
[16] *Ceramics International,* 46(4), 5050–5057. https://doi.org/10.1016/j.ceramint.2019.10.248
[17] A. Sobczak-Kupiec, Z. Wzorek. The influence of calcination parameters on free calcium oxide content in natural hydroxyapatite. *Ceramics International*, 2012, 38(1):641–647. https://doi.org/10.1016/j.ceramint.2011.06.065
[18] R.M. Albadr, S.A. Halfi, K.M. Ziadan. The effectiveness of oyster filler on the physical and mechanical properties of novel dental restorative composite. *AIP Conference Proceedings*, 2020, 2290(1): 050001. https://doi.org/10.1063/5.0031467
[19] Zhang, G. Y., Lin, R. S., & Wang, X. Y. (2023). Effect of waste oyster shell powder on the properties of alkali-activated slag-waste ceramic geopolymers. *Journal of Materials Research and Technology*, 22, 1768–1780. https://doi.org/10.1016/j.jmrt.2022.12.052
[20] Hu, C., Zhong, D., & Li, S. (2023). A study on effect of oyster shell powder on mechanical properties of asphalt and multiple degrees of modification mechanism. *Case Studies in Construction Materials*, 18, 01786. https://doi.org/10.1016/j.cscm.2022.e0178
[21] Ruslan, H. N., Muthusamy, K., Mohsin, S. M. S., Jose, R., & Omar, R. (2022). Oyster shell waste as a concrete ingredient: A review. Materials Today: *Proceedings*, 48, 713-719. https://doi.org/1 0.1016/j.matpr.2021.02.208
[22] Nayak, A., & Bhushan, B. (2021). Hydroxyapatite as an advanced adsorbent for removal of heavy metal ions from water: Focus on its applications and limitations. *Materials Today: Proceedings*, *46*, 11029–11034. https://doi.org/10.1016/j.matpr.2021.02.149
[23] Ibrahim, M., Labaki, M., Giraudon, J., & Lamonier, J. (2020). Hydroxyapatite, a multifunctional material for air, water and soil pollution control: A review. *Journal of Hazardous Materials*, *383*, 121139. https://doi.org/10.1016/j.jhazmat.2019.121139

[24] Balasooriya, I. L., Chen, J., Gedara, S. M. K., Han, Y., & Wickramaratne, M. N. (2022). Applications of Nano hydroxyapatite as adsorbents: A review. *Nanomaterials*, *12*(14), 2324. https://doi.org/10.3390/nano12142324
[25] Abdelraof, M., Farag, M. M., Al-Rashidy, Z. M., Ahmed, H. Y. A., El-Saied, H., & Hasanin, M. S. (2022). Green Synthesis of Bioactive Hydroxyapatite/Cellulose Composites from Food Industrial Wastes. *Journal of Inorganic and Organometallic Polymers and Materials*. https://doi.org/10.1007/s10904-022-02462-2
[26] Promsorn, T., Songsasen, A., & Wannalerse, B. (2021). Adsorption of Chromium (III) Solution Using Calcium Hydroxyapatite. *RMUTP Research Journal Sciences and Technology*, *15*(1), 91–104. https://doi.org/10.14456/jrmutp.2021.8
[27] Ahmed, H. Y., Safwat, N., Shehata, R., Althubaiti, E. H., Kareem, S., Atef, A., Qari, S. H., Aljahani, A. H., Al-Meshal, A. S., Youssef, M., & Sami, R. (2022). Synthesis of Natural Nano-Hydroxyapatite from Snail Shells and Its Biological Activity: Antimicrobial, Antibiofilm, and Biocompatibility. *Membranes*, *12*(4),
[28] 408. https://doi.org/10.3390/membranes12040408
[29] Shavandi, A., Bekhit, A. E. D. A., Ali, A., & Sun, Z. (2015). Synthesis of nano-hydroxyapatite (nHA) from waste mussel shells using a rapid microwave method. *Materials Chemistry and Physics*, *149*, 607-616.
[30] Aljaberi, K., AlBadr, R. M., & Ziadan, K. M. (2022). A new approach to prepare nano hydroxyapatite from oyster shells used for dental applications. *Journal of Kufa Physics*, 14(02), 35-46.
[31] K. Dhanaraj, G. Sures. (2018). Conversion of waste seashell (Anadara granosa) into valuable nanohydroxyapatite (nHAp) for biomedical applications. *Vacuum* 152 222-230.
[32] Amin Shavandi, Alaa El-Din A. Bekhit, Azam Ali, Zhifa Sun. (2014). Synthesis of nano-hydroxyapatite (nHA) from waste mussel shells using a rapid microwave method. *Materials Chemistry and Physics*,1-10
[33] Febrida, R., Setianto, S., Herda, E., Cahyanto, A., & Joni, I. M. (2021). Structure and phase analysis of calcium carbonate powder prepared by a simple solution method. *Heliyon*, *7*(11), e08344. https://doi.org/10.1016/j.heliyon.2021.e08344
[34] Niju, Subramania & Begum, Meera & Narayanan, Anantharaman. (2014). Modification of eggshell and its application in biodiesel production. *Journal of Saudi Chemical Society*. 10.1016/j.jscs.2014.02.010.
[35] Kifayah K. Thbayh, Rafid M. AlBadr, Kareema M. Ziadan. (2022). A new approach to prepare nano hydroxyapatite from oyster shells used for dental applications. *Journal of Kufa-Physics*. ISSN: 2077–5830
[36] Verwilghen, C., Chkir, M., Rio, S., Nzihou, A., Sharrock, P., & Depelsenaire, G. (2019). Convenient of Calcium Carbonate to Hydroxyapatite at Ambient Pressure. *Material Science and Engineering C,* 29, 771-773.
[37] Retrieved from http://dx.doi:10.1016/j.msec. 2018.07.007
[38] Rujitanapanich, S., Kumpapan, P., & Wanjanoi, P. (2014d). Synthesis of Hydroxyapatite from Oyster Shell via Precipitation. *Energy Procedia*, 56, 112–117. https://doi.org/10.1016/j.egypro.2014.07.138
[39] Recillas S., Rodriguez-Lugo V., Monttero ML, Viquez-Caro S.,Hernandez L., Castano VM. (2012). Studies on the precipitation behavior of calcium phosphare solutions. *Journal of Ceramic processing research,* 13, 5- 14.